Smyl, Danny; Bossuyt, Sven; Liu, Dong

Stacked elasticity imaging approach for visualizing defects in the presence of background inhomogeneity

Published in:
JOURNAL OF ENGINEERING MECHANICS: ASCE

DOI:
10.1061/(ASCE)EM.1943-7889.0001552

Published: 01/01/2019

Document Version
Peer-reviewed accepted author manuscript, also known as Final accepted manuscript or Post-print

Please cite the original version:
Smyl, D., Bossuyt, S., & Liu, D. (2019). Stacked elasticity imaging approach for visualizing defects in the presence of background inhomogeneity. *JOURNAL OF ENGINEERING MECHANICS: ASCE*, *145*(1), Article 06018006. https://doi.org/10.1061/(ASCE)EM.1943-7889.0001552

Stacked elasticity imaging approach for visualizing defects in the presence of background inhomogeneity

Article *in* Journal of Engineering Mechanics · July 2018

Danny Smyl
Aalto University

Dong Liu
University of Science and Technology of China

Stacked elasticity imaging approach for visualizing defects in the presence of background inhomogeneity

Danny Smyl[1], Sven Bossuyt[2], and Dong Liu[3]

[1]Postdoctoral Researcher, Department of Mechanical Engineering, Aalto University, Espoo, Finland. Email: danny.smyl@aalto.fi

[2]Associate Professor, Department of Mechanical Engineering, Aalto University, Espoo, Finland.

[3]Research Fellow, CAS Key Laboratory of Microscale Magnetic Resonance and Department of Modern Physics, University of Science and Technology of China (USTC), Hefei 230026, China. Email: dong2016@ustc.edu.cn

ABSTRACT

The ability to detect spatially-distributed defects and material changes over time is a central theme in structural health monitoring. In recent years, numerous computational approaches using electrical, electromagnetic, thermal, acoustic, optical, displacement, and other non-destructive measurements as input data for inverse imaging regimes have aimed to localize damage as a function of space and time. Often, these regimes aim to reconstruct images based off one set of data disregarding prior information from previous structural states. Here, we propose a stacked approach for one increasingly popular modality in structural health monitoring: Quasi-Static Elasticity Imaging. The proposed approach aims to simultaneously reconstruct spatial changes in elastic properties based on data from before and after the occurrence of damage in the presence of an inhomogeneous background. We conduct numerical studies, investigating in-plane plate stretching and bending, considering geometries with various damage levels. Results demonstrate the feasibility of the proposed imaging approach, indicating that the inclusion of prior information from multiple states visually improves reconstruction quality and decreases RMSE with respect to true images.

INTRODUCTION

The ability to visualize spatially-distributed defects, damage, and material changes in structures over time is critical in the assessment of structural health Balageas et al. (2010). Various computational approaches, such as Electrical Resistance Tomography (ERT) Tallman et al. (2017, 2015a,b); Hallaji et al. (2014); Yao and Soleimani (2012), Lamb/Guided-Wave methods Rodriguez et al. (2014); Hall and Michaels (2011); Gibson and Popovics (2005); Kessler et al. (2002), Digital Image Correlation Forsström et al. (2017); Lava et al. (2010); Pan et al. (2009), Thermal Imaging Ciang et al. (2008); Haj-Ali et al. (2008), X-ray Computed Tomography Buffiere et al. (2010); Ferrié et al. (2006); Schilling et al. (2005), Quasi-Static Elasticity Imaging (QSEI) Hoerig et al. (2017); Bonnet and Constantinescu (2005) and others have been successfully applied in imaging such processes. Often, computational approaches using any of the mentioned modalities aim to reconstruct images of structures based off one set of data corresponding to a single structural state. Such an approach does not directly utilize prior information from previous states, which is useful in reconstructing cases with complicated spatial distributions of damage Seppänen et al. (2017).

To take advantage of information contained in multiple data sets, researchers have developed schemes for reconstructing images on the basis of difference data, e.g. ERT with difference imaging Dai et al. (2016); Hallaji and Pour-Ghaz (2014). Difference imaging is a powerful tool for rapidly localizing damage since the reconstructions are commonly obtained using only one iteration Frerichs (2000). However, the results are often (i) qualitative due to linearization Smyl et al. (2016) and (ii) offer little information information on background inhomogeneity, since reconstructions are computed from differences in measured data sets Vauhkonen (1997). For quantitative imaging of multiple structural states, a non-linear approach should be taken.

By re-parameterizing (stacking) the ERT inverse problem, it was shown in Liu et al. (2016); Mozumder et al. (2015); Liu et al. (2015) that multiple states may be simultaneously reconstructed via the inclusion of prior information in regularization terms for each state (compound regularization). Specifically, smoothness-promoting regularization was utilized for the initial state and Total Variation (TV) regularization was used for reconstructing sharp changes in the second state.

The use of TV in applications detecting sharp features is well-established, as demonstrated in, e.g., structural crack detection Seppänen et al. (2017); Hallaji et al. (2014), organ boundary identification Borsic et al. (2010), and geophysical applications Alrajawi et al. (2017). Using realizations related to the problem physics, the authors of Liu et al. (2016, 2015) employed multiple constraints on each state which improved reconstruction quality and convergence behavior during the minimization scheme.

In this work, we are motivated by these recent developments in inverse-problems and we aim to apply stacking techniques to QSEI. The modality considered herein, QSEI, is an inverse method that numerically reconstructs the distribution of elastic modulus based off displacement field data. While QSEI is most commonly used for medical imaging of tissue abnormalities Papadacci et al. (2017), some works have applied QSEI to structural health monitoring, e.g. Hoerig et al. (2017); Bonnet and Constantinescu (2005). Recent algorithmic advances for medical QSEI using adjoint and non-linear methods Goenezen et al. (2011); Gokhale et al. (2008); Oberai et al. (2003, 2004) further encourage the use of QSEI in structural health monitoring. In this article, we begin by presenting classical and stacked QSEI reconstruction approaches. Following, we conduct a numerical investigation, comparing reconstructions using both approaches for in-plane plate bending and stretching. Lastly, discussion and conclusions are presented.

CLASSICAL AND STACKED QSEI

Classical approach

The classical aim of QSEI is to determine the distribution of the inhomogeneous elastic modulus E using displacement field data u_m, knowledge of the structural geometry, and loading. In practice, u_m may be obtained experimentally using optical methods, such as Digital Image Correlation (DIC). Formally, the classical QSEI Least-Squares (LS) inverse problem is stated in the following: Given distributed displacement data u_m, structural geometry Ω, boundary information $\partial\Omega$, and external forces f, determine E. The observation model for the classical QSEI description is then:

$$u_m = U(E) + e \tag{1}$$

where $U(E)$ are the simulated displacements and e is Gaussian-distributed noise. The LS solution based on this observation model is written as:

$$\ell_c = \underset{E>0}{\operatorname{argmin}} ||L_e(u_m - U(E))||^2 + p_E(E) \tag{2}$$

where $p_E(E)$ is the regularization functional, $L_e^T L_e = C_e^{-1}$ where C_e is the observation noise covariance matrix, $||\cdot||$ denotes the Euclidean norm, and the subscript "c" denotes "classical." The regularization term is included due to the ill-posed nature of the inverse problem, meaning that standard LS approaches may yield non-unique solutions. Commonly, $U(E)$ is solved using the Finite Element Method (FEM) Goenezen et al. (2011). In this work, the FEM is also employed using piece-wise linear triangular elements assuming incompressible isotropic plane-stress conditions. Symbolically, the forward model is written as

$$U_j = \sum_{i=1}^{N_n} K_{ji}^{-1} f_i \tag{3}$$

where N_n is the total number of unknown displacements and K_{ji}^{-1} and f_i are often referred to and the compliance matrix and force vector, respectively Surana and Reddy (2016).

Because we are interested in reconstructing structural configurations with smoothly-correlated background inhomogeneity (i.e., the distribution of E in an undamaged state), edge-preserving regularization, such as TV, is not used here in the *classical* approach. Therefore, we select smoothness-promoting regularization for $p_E(E)$, which is given by

$$p_E(E) = ||L_E(E - E_{\text{exp}})||^2 \tag{4}$$

where L_E is a spatially-weighted matrix and E_{exp} is the expected value of E computed by solving the best homogeneous estimate $E_{\text{exp}} = \operatorname{argmin}||u_m - U(E)||^2$.

The optimization problem is solved iteratively using a Gauss-Newton (GN) scheme equipped with a line-search algorithm to determine the step size Δ_k in the parameterized solution $\theta_k = \theta_{k-1} + \Delta_k \bar{\theta}$ where θ_k is the current estimate and $\bar{\theta}$ is the LS update. Such an approach requires the

Jacobian $J = \frac{\partial U}{\partial E}$ at each iteration k, which is computed using the perturbation method with central differencing, where each entry is computed using

$$J_{ij} = \frac{U(E_{k-1} + \Delta^J) - U(E_{k-1} - \Delta^J)}{2\Delta^J} \tag{5}$$

where the perturbation Δ^J is computed as a function of the double-precision of the machine ϵ using $\Delta^J = \sqrt[3]{\frac{\epsilon}{2}}$ following An et al. (2011). We note that the majority of the computing time is spent calculating J; other gradient-based algorithms may be more efficient Oberai et al. (2003). However, the GN scheme was selected due to its fast convergence behavior. The stopping criteria used in all estimates was $\varphi = (\ell_k - \ell_{k-5})/\ell_{k-5} \leq 10^{-3}$, where ℓ denotes the cost function for a given reconstruction approach. The selection of $\varphi = \varphi(\ell_k, \ell_{k-5})$ was made to ensure that the optimization was stopped at a stable minimum, especially in cases where the objective function may have small fluctuations. This criteria was originally used in Oberai et al. (2004) and was found to be satisfactory herein.

Stacked approach

In the stacked approach, we have the following model considering both the initial E_1 and final state E: $E_1 + \delta E = E$, where δE is the change between states. Here, we make the simplifying assumption that damage decreases E (i.e. $\delta E \leq 0$), which is realistic in the case of, for example, localized cracking or corrosion Seppänen et al. (2017). In the case of a through-crack, $E = 0$ can reasonably be assumed within the crack. We also remark that for such a model to be physically realistic, neither E nor E_1 can be negative. Based on this observation model, we may concatenate measurements from two states (undamaged (u_1) and damaged (u_2)) in the following

$$\underbrace{\begin{bmatrix} u_1 \\ u_2 \end{bmatrix}}_{\overline{u_m}} = \underbrace{\begin{bmatrix} U(E_1) \\ U(E_1 + \delta\sigma) \end{bmatrix}}_{\overline{U}(\bar{E})} + \underbrace{\begin{bmatrix} e_1 \\ e_2 \end{bmatrix}}_{\overline{e}} \tag{6}$$

where $\overline{e} = [e_1, e_2]^T$ is the concatenated noise vector. Based on the physical realizations that (i)

$\delta E \leq 0$, (ii) E_1 and E are non-negative, and using Eq. 6, we may then write the regularized LS solution, with subscript "s" denoting "stacking," as

$$\ell_s = \arg \min_{\substack{E_1>0 \\ E>0 \\ \delta E \leq 0}} \{||\bar{L}_{\bar{e}}(\overline{u_m} - \overline{U}(\bar{E}))||^2 + p(\bar{E})\} \tag{7}$$

where $\bar{L}_{\bar{e}}^T \bar{L}_{\bar{e}} = \bar{C}_e$ uses the block form of the stationary noise covariance matrix (i.e $C_{e_1} = C_{e_2} = C_e$) which is written as $\bar{C}_e = \begin{bmatrix} C_{e_1} & \mathbf{0} \\ \mathbf{0} & C_{e_2} \end{bmatrix}$. Moreover, $p(\bar{E}) = p_1(E_1) + p_2(\delta E)$ is the compound regularization term using Eq. 4 for the smoothly-correlated E_1 and TV regularization for δE, given by

$$p_2(\delta E) = \alpha \sum_{q=1}^{N_e} \sqrt{||(\nabla \delta E)|_{e_q}||^2 + \beta} \tag{8}$$

where α is a TV weighting parameter, $\nabla \delta E|_{e_q}$ is the gradient of δE at element e_q, β is a stabilization parameter, and N_e is the number of elements in the discretization. In selecting α, $\alpha = -\frac{\ln(1-\frac{p_\alpha}{100})}{E_{1,\exp}/d}$ is employed, where p_α is the % confidence that values of δE lie between $[-E_{1,\exp}, 0]$ and d is the FEM element width. Moreover, the criteria $\beta = \zeta(\frac{E_{1,\exp}}{d})^2$ was used in computing the stabilization parameter. The selection of TV parameters were chosen following González et al. (2017); $p_\alpha = 90.0$ and $\zeta = 10^{-5}$ were used in all reconstructions.

The stacked approach also employed a GN-based minimization scheme, which requires the concatenated Jacobian written as follows

$$J_{\overline{U}}(\bar{E}) = \begin{bmatrix} J_U(E_1) & \mathbf{0} \\ J_U(E_1 + \delta E) & J_U(E_1 + \delta E) \end{bmatrix}. \tag{9}$$

We note that all constraints were handled using the interior point method.

NUMERICAL INVESTIGATION

We investigated two structural geometries using the classical and stacked reconstruction approaches. Two structural cases are considered: case (a) plate stretching and case (b) in-plane plate bending (herein referred to as "plate bending"). In both cases, the structures have randomized "blob-like" background distributions of elasticity modulus and a Poisson ratio $\nu = 0.35$. The range of material properties used simulated a compliant structural material with 25.0 GPa $< E <$ 50.0 GPa. The structures of interest, boundary conditions, loading conditions, and meshing are provided in Fig. 1. Out of plane deformations were not considered. For each geometry, two levels of structural damage are considered with η =1.0 and 2.0% noise standard deviation added to simulated measurement values u_m and $\overline{u_m}$.

We begin by investigating case (a). Results are shown in Fig. 2, reporting all stacked estimates ($E_1 + \delta E = E$) as well as the classical reconstruction estimate E_c. As a whole, the proposed stacked approach captured all estimated quantities. Visually, it is apparent that the stacked approach better estimated both background elastic modulus distribution and damage levels I and II than the classical reconstruction approach (this claim will be quantified in the following section). This is anticipated result, as the regularization functional used in the classical approach is not appropriate for simultaneous reconstruction of a smooth background and a sharp change in E. Moreover, as expected, images with a higher noise level, $\eta = 2.0$, were visually more blurry using both approaches.

It is interesting to note that all reconstructions of E_1 are over-smoothed and overestimated with respect to the true distributions. This is a consequence of the ill-posed nature of the inverse problem and the measurement sensitivity to smooth changes in E. In damage level II, however E_1 is better estimated. This illuminates one weakness in the stacked reconstruction method: the relative "weighting" between E_1 and δE during minimization of Eq. 7. Indeed, in damage level II, where δE is more spatially-distributed, the "weight" of δE is higher, leading to a better visualization of both E_1 and E relative to Damage Level I. This may be compensated, for example by optimizing the value of α in Eq. 8 or improving constraints in Eq. 7 using prior information related to E_1.

We now consider case (b), reconstructions for this case are shown in Fig. 3. As a whole, the stacked approach well reconstructs the damage patterns, although the aforementioned issues with E_1 in case (a) are also observed here. Visually, it is clear that classical reconstructions underestimate the size of the ellipsoidal damage (damage level I), while stacking reconstructions overestimate the size of the ellipsoidal damage. Overall, the reconstruction quality in stacked and classical approaches are visually comparable for damage level I. This similarity in reconstruction quality results from the large size of the damage area located in a region with low gradients in the background elasticity distribution. This is a favorable condition for reconstruction approaches using smoothness-promoting regularization Kaipio and Somersalo (2007); Vauhkonen et al. (1998).

On the other hand, in damage level II, the locations of distributed damages are in regions with both low and high gradients of the background elasticity distribution. While the presence of large background fluctuations did not affect the localization of damages, the magnitude of the distributed damages are poorly estimated using the classical approach. Owing to the improved robustness of the stacked approach, allowing for both sharp fluctuations in δE and smoothness in E_1, the magnitude of E in the damaged regions is well estimated. In the following section, we further examine the visual observations of this section in a quantitative analysis of the reconstructions.

DISCUSSION

Reconstructions comparing E for the classical and stacked approaches were reported in the previous section. However, while there were notable visual improvements in reconstructions of E when employing the stacked approach, the degree of improvement was subtle and not immediately apparent. To quantify the visual observations from the last section, i.e. that the stacking approach better reconstructed E, we compare the root mean square error (RMSE = $\sqrt{\sum_{l=1}^{N_e}(E_{\text{true},l} - E_l)^2/N_e}$) for all reconstructions. The RMSEs for all cases are presented in Fig. 4 as a function of the noise level $\eta = 1.0$ and 2.0%.

Fig. 4 confirms the visual observations from the previous sections. The RMSEs for stacked reconstructions in both cases are lower than those of the classical reconstructions. This indicates that the stacked approach better reconstructed the true elasticity distributions. Interestingly, both reconstruction approaches followed the same trend for a given case. In plate bending, the RMSEs are shown to increase as the damage level increases. The contrary is observed for plate stretching.

One possible explanation for this observation is the sensitivity of QSEI to the displacement field. The location of the large ellipsoid in plate bending damage level I is towards the top of the beam. In this configuration, the bending stresses, and therefore displacements, are highest with respect to the fixed x-axis location. However, in plate bending damage level II the localized damages are smaller, with one localized damage in the center – where bending stresses are lowest. This explains the poor visibility of the central inclusion for classical reconstructions in Fig. 3

Reconstructions of plate stretching also show sensitivity to the displacement field. Since damage level II is more distributed than damage level I – particularity in the vertical direction – the displacement field is less locally disturbed, thereby offering better global displacement information. This had a significant effect on RMSE in classical reconstructions of plate stretching, while only subtly affecting the RMSE of stacked reconstructions.

While the stacked approach was shown to decrease the RMSE of reconstructions relative to the classical approach, the primary advantages of the stacked approach are primarily (i) better prior information incorporated through compound regularization, (ii) employment of multiple constraints on E_1, δE, and E using physical realizations related to damage processes, and (iii) the use of multiple data sets in reconstructing $E = E_1 + \delta E$. Additional flexibility and improvement on the present stacking approach may also be incorporated by including, e.g., upper constraints on E_1 and E using prior knowledge of the material, different forms of regularization based on the expected distributions of δE and E, and different noise models for each state accounting for non-Gaussian statistics. We remark here, however, that some weaknesses in the stacking approach were identified. Namely, over-smoothing and overestimation of E_1 which had a compound effect via the degradation of δE reconstructions. Improved selection of the TV parameter α and prior knowledge of the problem's constraints should alleviate these weaknesses.

Concerning point (iii), we would like to mention that the classical model may also be used in a dual model to estimate multiple states. For example, one may reconstruct E_1 and E separately and estimate $\delta E = E - E_1$. This dual problem was examined in a preliminary study. However, results for $\delta E = E - E_1$ were often unrealistic, taking both positive and negative values. This results from the fact that the dual problem is insufficiently constrained and not parameterized such that $\delta E \leq 0$

and $E = E_1 + \delta E$ are guaranteed. In cases where the user is only interested in damage localization, such an approach may be suitable. For situations that require quantitative results, use of either classic (single state) estimation of E or the stacked model should be used.

In summary, the results presented herein support the feasibility of the proposed stacked model, given the improved performance with respect to the classical approach. We note that experimentally-obtained displacement measurements are required to validate the field performance of the stacking approach. In future works, we aim to (i) utilize experimental displacement fields obtained using Digital Image Correlation in a coupled DIC/QSEI regime targeted at characterizing orthotropic elastic properties and detecting damage in carbon fiber reinforced polymer (CFRP) elements and (ii) develop a joint DIC/QSEI reconstruction approach for characterizing micro-structural elastic features of metallic materials and for localizing damage in large composite structures.

CONCLUSIONS

In this work we proposed a new stacked approach for QSEI of structures in the presence of background inhomogeneity. The proposed stacked approach was parameterized such that two structural states may be imaged simultaneously. The primary advantages of this approach were noted: (i) incorporation of prior information related to each structural state and (ii) implementation of constraints based on physical realizations related to each state. To test the reconstruction regime, numerical studies were conducted. In-plane plate stretching and bending were investigated considering several localized and distributed damage configurations. The proposed approach was corroborated with a classical QSEI approach. Following, a discussion was provided.

The results of the numerical study support the feasibility of the stacked reconstruction approach. In all cases, it was shown that the stacked approach outperforms the classical approach based off visual observation and analysis of reconstructions' RMSEs. Future work using experimentally-obtained displacement measurements is required to validate the field performance of the stacked approach. Planned work in the near future will investigate the use of coupled QSEI/DIC approaches for characterizing orthotropic elastic properties and damage in CFRP elements. In the more distant future, we aim to develop a joint QSEI/DIC framework for complimentary imaging of damage and characterization of materials/structures at micro and macro scales.

ACKNOWLEDGMENTS

Authors DS and SB would like to acknowledge the support of the Department of Mechanical Engineering at Aalto University throughout this project. Aalto University Science-IT provided the computing platform for this work on the Aalto Triton cluster, this support is greatly acknowledged. DL was supported by Anhui Provincial Natural Science Foundation (1708085MA25).

REFERENCES

Alrajawi, M., Siahkoohi, H., and Gholami, A. (2017). "Inversion of seismic arrival times with erratic noise using robust tikhonov–tv regularization." *Geophysical Journal International*, 211(2), 853–864.

An, H.-B., Wen, J., and Feng, T. (2011). "On finite difference approximation of a matrix-vector product in the jacobian-free newton–krylov method." *Journal of Computational and Applied Mathematics*, 236(6), 1399 – 1409.

Balageas, D., Fritzen, C.-P., and Güemes, A. (2010). *Structural health monitoring*, Vol. 90. John Wiley & Sons.

Bonnet, M. and Constantinescu, A. (2005). "Inverse problems in elasticity." *Inverse Problems*, 21(2), R1.

Borsic, A., Graham, B. M., Adler, A., and Lionheart, W. R. (2010). "In vivo impedance imaging with total variation regularization." *IEEE Transactions on Medical Imaging*, 29(1), 44–54.

Buffiere, J.-Y., Maire, E., Adrien, J., Masse, J.-P., and Boller, E. (2010). "In situ experiments with X-ray tomography: an attractive tool for experimental mechanics." *Experimental Mechanics*, 50(3), 289–305.

Ciang, C. C., Lee, J.-R., and Bang, H.-J. (2008). “Structural health monitoring for a wind turbine system: a review of damage detection methods.” *Measurement Science and Technology*, 19(12), 122001.

Dai, H., Gallo, G. J., Schumacher, T., and Thostenson, E. T. (2016). “A novel methodology for spatial damage detection and imaging using a distributed carbon nanotube-based composite sensor combined with electrical impedance tomography.” *Journal of Nondestructive Evaluation*, 35(2), 26.

Ferrié, E., Buffiere, J.-Y., Ludwig, W., Gravouil, A., and Edwards, L. (2006). “Fatigue crack propagation: In situ visualization using X-ray microtomography and 3D simulation using the extended finite element method.” *Acta Materialia*, 54(4), 1111–1122.

Forsström, A., Luumi, L., Bossuyt, S., and Hänninen, H. (2017). “Localisation of plastic deformation in friction stir and electron beam copper welds.” *Materials Science and Technology*, 33(9), 1119–1129.

Frerichs, I. (2000). “Electrical impedance tomography (EIT) in applications related to lung and ventilation: a review of experimental and clinical activities.” *Physiological measurement*, 21(2), R1.

Gibson, A. and Popovics, J. S. (2005). “Lamb wave basis for impact-echo method analysis.” *Journal of Engineering Mechanics*, 131(4), 438–443.

Goenezen, S., Barbone, P., and Oberai, A. A. (2011). “Solution of the nonlinear elasticity imaging inverse problem: The incompressible case.” *Computer Methods in Applied Mechanics and Engineering*, 200(13), 1406–1420.

Gokhale, N. H., Barbone, P. E., and Oberai, A. A. (2008). “Solution of the nonlinear elasticity imaging inverse problem: the compressible case.” *Inverse Problems*, 24(4), 045010.

González, G., Kolehmainen, V., and Seppänen, A. (2017). "Isotropic and anisotropic total variation regularization in electrical impedance tomography." *Computers & Mathematics with Applications*.

Haj-Ali, R., Wei, B.-S., Johnson, S., and El-Hajjar, R. (2008). "Thermoelastic and infrared-thermography methods for surface strains in cracked orthotropic composite materials." *Engineering Fracture Mechanics*, 75(1), 58–75.

Hall, J. S. and Michaels, J. E. (2011). "Computational efficiency of ultrasonic guided wave imaging algorithms." *IEEE Transactions on Ultrasonics, Ferroelectrics, and Frequency Control*, 58(1).

Hallaji, M. and Pour-Ghaz, M. (2014). "A new sensing skin for qualitative damage detection in concrete elements: Rapid difference imaging with electrical resistance tomography." *NDT & E International*, 68, 13–21.

Hallaji, M., Seppänen, A., and Pour-Ghaz, M. (2014). "Electrical impedance tomography-based sensing skin for quantitative imaging of damage in concrete." *Smart Materials and Structures*, 23(8), 085001.

Hoerig, C., Ghaboussi, J., and Insana, M. F. (2017). "An information-based machine learning approach to elasticity imaging." *Biomechanics and Modeling in Mechanobiology*, 16(3), 805–822.

Kaipio, J. and Somersalo, E. (2007). "Statistical inverse problems: discretization, model reduction and inverse crimes." *Journal of Computational and Applied Mathematics*, 198(2), 493–504.

Kessler, S. S., Spearing, S. M., and Soutis, C. (2002). "Damage detection in composite materials using lamb wave methods." *Smart Materials and Structures*, 11(2), 269.

Lava, P., Cooreman, S., and Debruyne, D. (2010). "Study of systematic errors in strain fields obtained via dic using heterogeneous deformation generated by plastic fea." *Optics and Lasers in Engineering*, 48(4), 457–468.

Liu, D., Kolehmainen, V., Siltanen, S., Laukkanen, A., and Seppänen, A. (2015). "Estimation of conductivity changes in a region of interest with electrical impedance tomography." *Inverse Problems and Imaging*, 9(1), 211–229.

Liu, D., Kolehmainen, V., Siltanen, S., Laukkanen, A.-M., and Seppänen, A. (2016). "Nonlinear difference imaging approach to three-dimensional electrical impedance tomography in the presence of geometric modeling errors." *IEEE Transactions on Biomedical Engineering*, 63(9), 1956–1965.

Mozumder, M., Tarvainen, T., Seppänen, A., Nissilä, I., Arridge, S. R., and Kolehmainen, V. (2015). "Nonlinear approach to difference imaging in diffuse optical tomography." *Journal of Biomedical Optics*, 20(10), 105001–105001.

Oberai, A. A., Gokhale, N. H., Doyley, M. M., and Bamber, J. C. (2004). "Evaluation of the adjoint equation based algorithm for elasticity imaging." *Physics in Medicine and Biology*, 49(13), 2955.

Oberai, A. A., Gokhale, N. H., and Feijóo, G. R. (2003). "Solution of inverse problems in elasticity imaging using the adjoint method." *Inverse Problems*, 19(2), 297.

Pan, B., Qian, K., Xie, H., and Asundi, A. (2009). "Two-dimensional digital image correlation for in-plane displacement and strain measurement: a review." *Measurement Science and Technology*, 20(6), 062001.

Papadacci, C., Bunting, E. A., and Konofagou, E. E. (2017). "3d quasi-static ultrasound elastography with plane wave in vivo." *IEEE Transactions on Medical Imaging*, 36(2), 357–365.

Rodriguez, S., Deschamps, M., Castaings, M., and Ducasse, E. (2014). "Guided wave topological imaging of isotropic plates." *Ultrasonics*, 54(7), 1880–1890.

Schilling, P. J., Karedla, B. R., Tatiparthi, A. K., Verges, M. A., and Herrington, P. D. (2005). "X-ray computed microtomography of internal damage in fiber reinforced polymer matrix composites." *Composites Science and Technology*, 65(14), 2071–2078.

Seppänen, A., Hallaji, M., and Pour-Ghaz, M. (2017). "A functionally layered sensing skin for the detection of corrosive elements and cracking." *Structural Health Monitoring*, 16(2), 215–224.

Smyl, D., Hallaji, M., Seppänen, A., and Pour-Ghaz, M. (2016). "Three-dimensional electrical impedance tomography to monitor unsaturated moisture ingress in cement-based materials." *Transport in Porous Media*, 115(1), 101–124.

Surana, K. S. and Reddy, J. (2016). *The Finite Element Method for Boundary Value Problems: Mathematics and Computations*. CRC Press.

Tallman, T., Gungor, S., Koo, G., and Bakis, C. (2017). "On the inverse determination of displacements, strains, and stresses in a carbon nanofiber/polyurethane nanocomposite from conductivity data obtained via electrical impedance tomography." *Journal of Intelligent Material Systems and Structures*, 28(18), 2617–2629.

Tallman, T., Gungor, S., Wang, K., and Bakis, C. (2015a). "Tactile imaging and distributed strain sensing in highly flexible carbon nanofiber/polyurethane nanocomposites." *Carbon*, 95, 485–493.

Tallman, T. N., Gungor, S., Wang, K., and Bakis, C. E. (2015b). "Damage detection via electrical impedance tomography in glass fiber/epoxy laminates with carbon black filler." *Structural Health Monitoring*, 14(1), 100–109.

Vauhkonen, M. (1997). "Electrical impedance tomography and prior information.

Vauhkonen, M., Vadasz, D., Karjalainen, P. A., Somersalo, E., and Kaipio, J. P. (1998). "Tikhonov regularization and prior information in electrical impedance tomography." *IEEE Transactions on Medical Imaging*, 17(2), 285–293.

Yao, A. and Soleimani, M. (2012). "A pressure mapping imaging device based on electrical impedance tomography of conductive fabrics." *Sensor Review*, 32(4), 310–317.

List of Figures

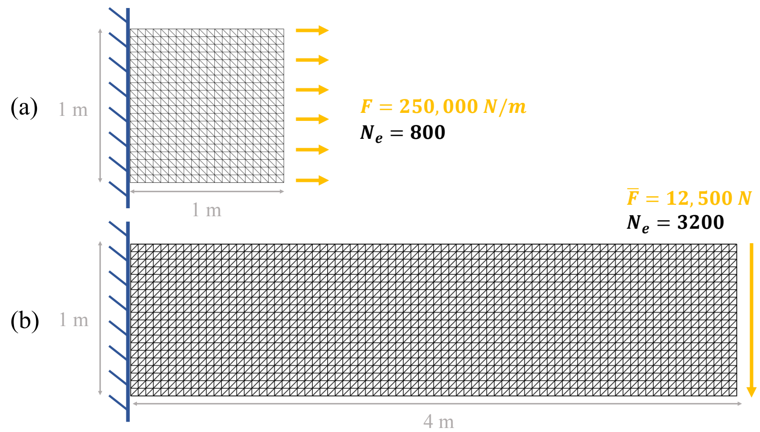

Fig. 1. Schematic illustration of structural geometries, loading conditions, boundary conditions, and FEM meshes. Case (a) stretched plate with fixed left end: 250,000 N/m load evenly distributed among right side nodes and case (b) plate bending with fixed left end: 12,500 N shear load evenly distributed among right side nodes. Each geometry has a maximum element dimension of 5.0 cm. The thickness of the stretched plate and bent plates are 1.0 and 2.5 cm, respectively.

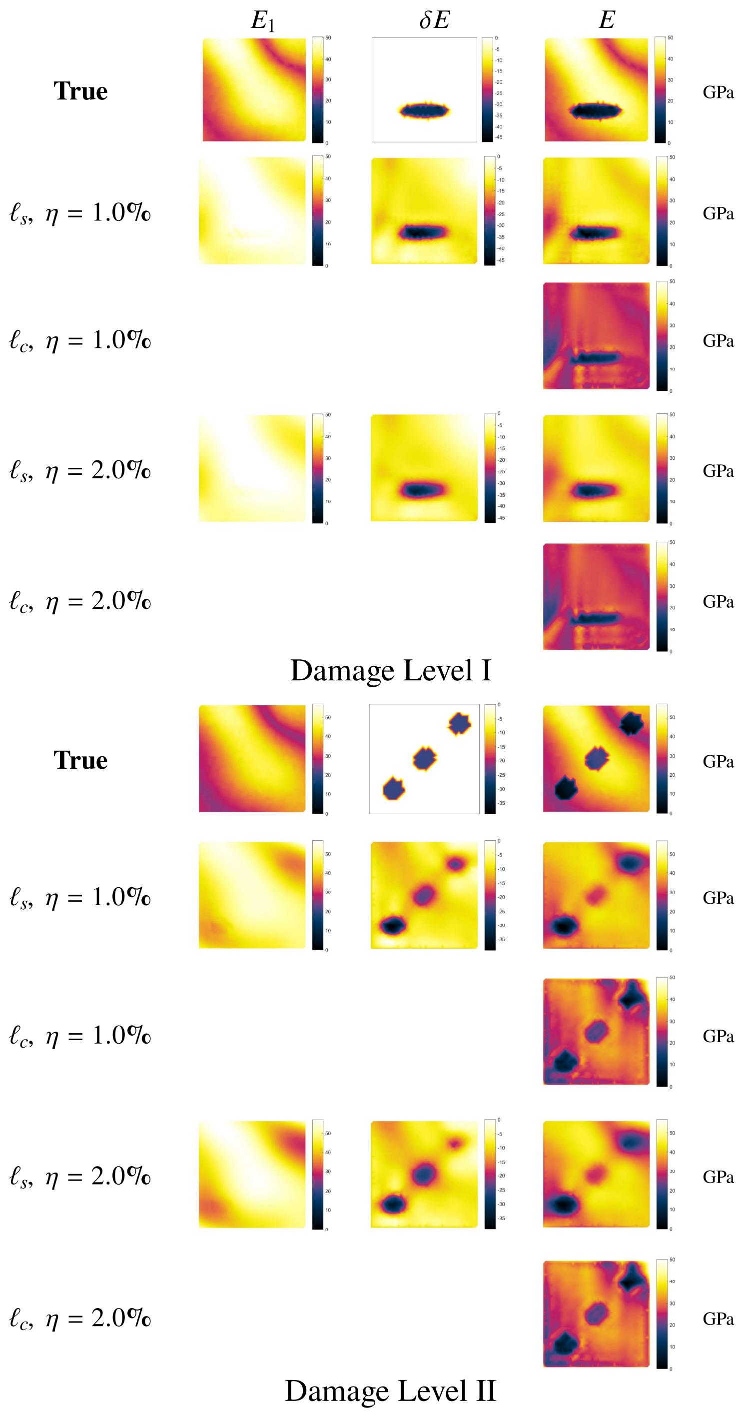

Fig. 2. Stacked ($E_1 + \delta E = E$) and classical (E) reconstructions of ellipsoidal (Damage Level I) and distributed damages (Damage Level II) in a stretched plate in the presence of background inhomogeneity. The far left column, column 1, designates the reconstruction type (ℓ_s, stacked and ℓ_c, classical) with the data noise level, η; column 2 contains stacked reconstructions of E_1; column 3 contains stacked reconstructions of δE; and column 4 contains classical and stacked reconstructions of E.

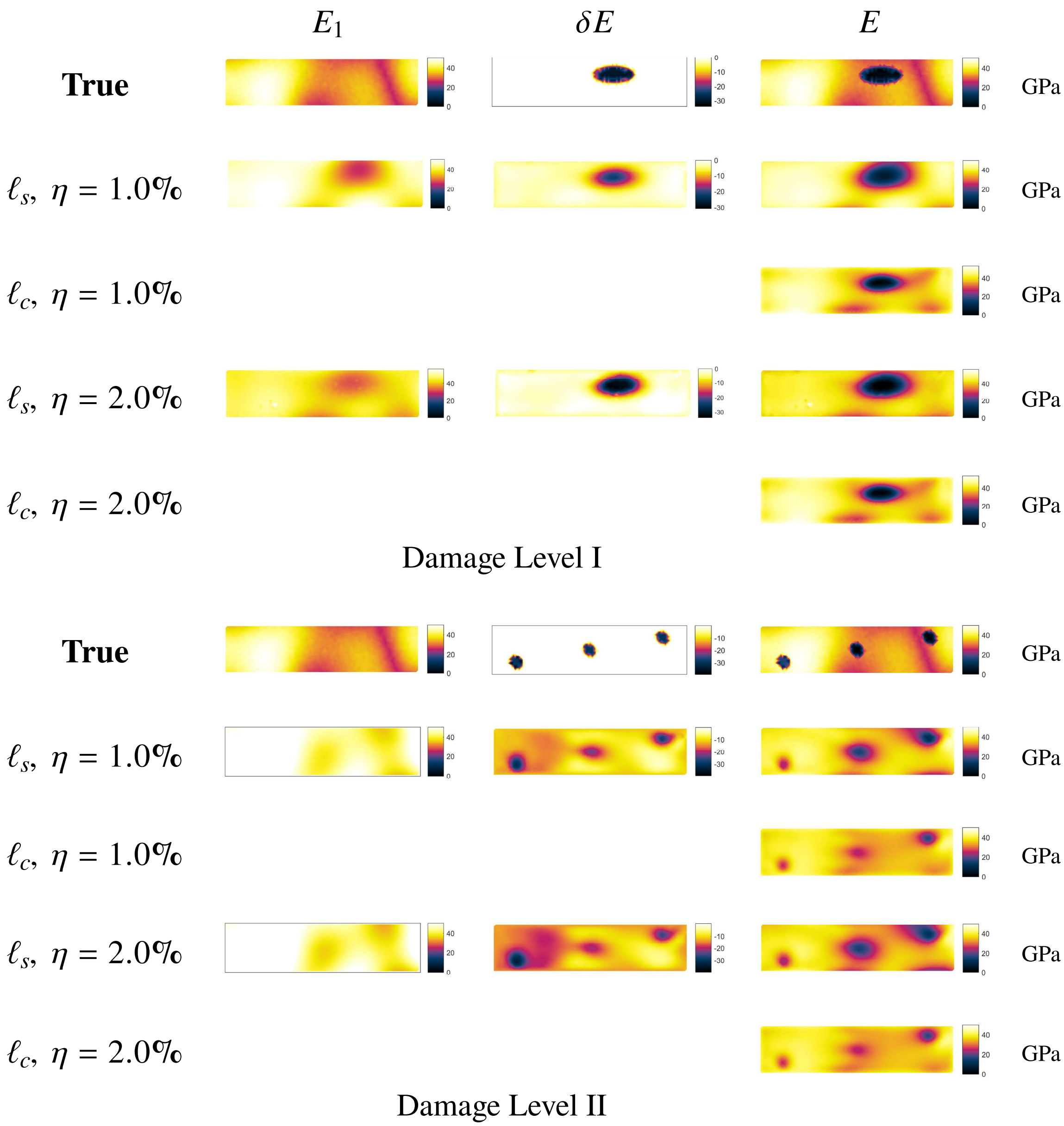

Fig. 3. Stacked ($E_1 + \delta E = E$) and classical (E) reconstructions of ellipsoidal (Damage Level I) and distributed damages (Damage Level II) in a bent beam in the presence of background inhomogeneity. The far left column, column 1, designates the reconstruction type (ℓ_s, stacked and ℓ_c, classical) with the data noise level, η; column 2 contains stacked reconstructions of E_1; column 3 contains stacked reconstructions of δE; and column 4 contains classical and stacked reconstructions of E.

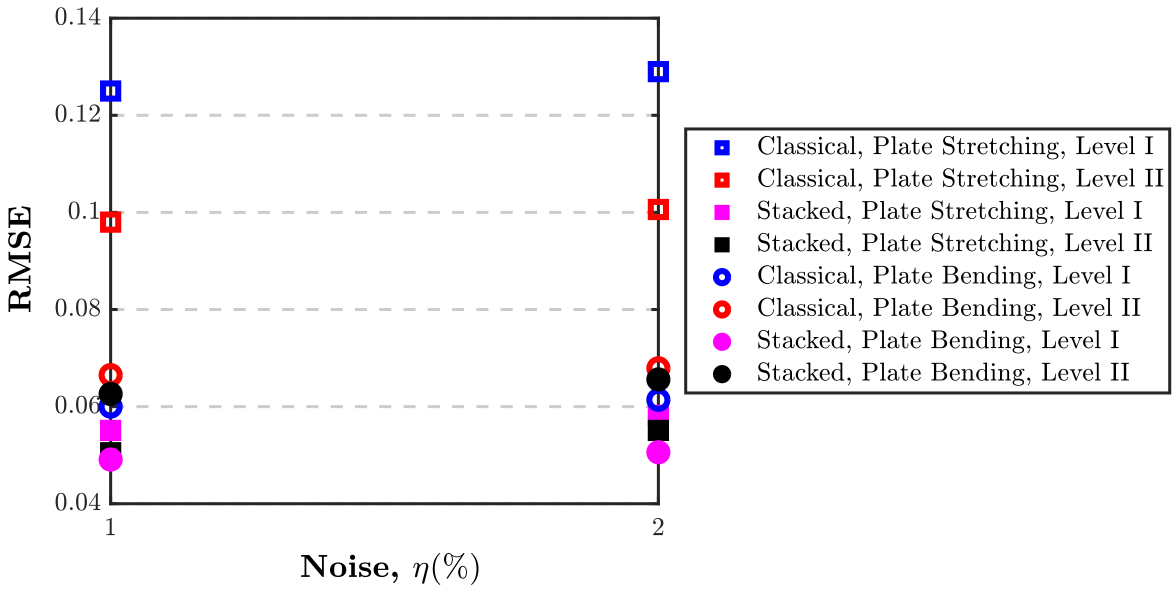

Fig. 4. RMSEs of E reconstructions for plate bending and stretching considering two damage levels (I and II) and added noise η = 1.0 and 2.0% using classical and stacked approaches. Square and round markers indicate plate stretching and bending, respectively. Solid markers and hollow markers indicate stacked and classical reconstructions, respectively.